

Bias Corrected PSD Estimation for an Adaptive Array With Moving Interference

Brian D. Jeffs, *Senior Member, IEEE*, and Karl F. Warnick, *Senior Member, IEEE*

Abstract—We address the issue of computing power spectral density (PSD) estimates at the output of a beamforming sensor array in the presence of strong moving interference. It is shown that the time-varying spatial response of an adaptive beamformer (“pattern rumble”) causes estimation bias in the PSD of both the signal of interest (SOI) and noise. In applications such as radio astronomy with stringent sensitivity requirements, even small pattern variations can be problematic because the resulting higher variance noise spectrum estimates make it impossible to detect signals of interest which are many decibels below the noise floor. Distortion in beam mainlobe shape also introduces errors in SOI direction estimates. To overcome this problem, an extension of the method described in Leshem *et al.*, 2000, is developed which eliminates pattern-distortion-induced PSD bias and spatial response errors over the long-term PSD averaging window. Both simulated and real data experiments demonstrate algorithm effectiveness in realizing an undistorted effective (average) beam spatial response while maintaining a low noise floor level. This algorithm will enable PSD estimation using multi-antenna sensors and adaptive interference cancellation for radio astronomy, remote sensing, and other sensitive radiometry applications where cancellation has not been feasible.

Index Terms—Adaptive arrays, interference suppression, radio astronomy, spectral analysis, space–time adaptive processing (STAP).

I. INTRODUCTION

THIS paper considers the problem of using a sensor array for nonparametric temporal power spectral density (PSD) estimation of a weak signal of interest (SOI) in the presence of background noise and strong moving interference. It is assumed that the SOI direction of arrival is known and that the spatial spectrum of the scene is not of interest beyond any necessary estimation required to remove the interference. It may also be necessary to obtain an accurate estimate of the noise field PSD (not including interference) in order to separate it from the SOI PSD, as described below. This scenario is common in radio astronomy (RA) where the goal is often to observe the spectral properties of a faint deep-space object at a fixed direction and in a harsh signal environment, and in passive remote sensing, where radiometric measurements are used to infer physical properties of a distant scene.

Manuscript received Jun. 7, 2007; revised January 3, 2008. The associate editor coordinating the review of this manuscript and approving it for publication was Hongbin Li. This work was funded by the National Science Foundation under Grant AST-0352705. A preliminary partial version of this work appeared in the Proceedings of the IEEE International Conference on Acoustics, Speech, and Signal Processing, Honolulu, HI, April 2007.

The authors are with the Department of Electrical and Computer Engineering, Brigham Young University, Provo, UT 84602 USA (e-mail: bjeffs@ee.byu.edu; warnick@ee.byu.edu).

Digital Object Identifier 10.1109/TSP.2008.919637

In the broad sense this problem falls into the category of space–time adaptive processing (STAP) since both spatial and temporal samples are used to estimate signal parameters of interest [5], [6]. Due to the extremely low signal levels in typical radiometric measurements, mainstream STAP algorithms used for radar and wireless communications applications are not suitable here. We will also not undertake to develop an optimal temporal-spatial estimator (e.g., in the ML sense) for the SOI PSD. Rather, for practical reasons the development will consider an architecture which separates the spatial and temporal processing into distinct adaptive beamforming and PSD estimation steps as illustrated in Fig. 1. We will discuss how this configuration inevitably leads to PSD estimation bias in the presence of non-stationary interference and noise. We then develop a bias correction method which integrates the spatial and temporal processing into a joint estimator which eliminates spectral corruption caused by adaptive interference cancellation.

One could use many candidate adaptive beamforming algorithms for interference nulling in the architecture of Fig. 1. However, interference cancellation of necessity introduces variation or distortion in the beamforming spatial pattern, particularly as interference encroaches on the beam mainlobe [7]–[9]. It will be shown analytically in Section III-B and experimentally in Section IV that these beampattern distortions bias the SOI PSD estimate.

In RA observation, the array in Fig. 1 may represent a planar array of antennas at the focal plane of a large parabolic reflector telescope dish. Array feeds are currently an active area of research for radio astronomy because they offer the possibility of adaptive interference cancellation while forming multiple simultaneous beams in different look directions near the dish’s primary axis, and improved control over the dish illumination pattern to reduce spillover noise as compared to conventional horn feeds [10]–[16]. No operating radio telescope currently uses a beamforming array feed in an adaptive interference cancellation mode. This is despite the fact that ubiquitous and troublesome man-made interference often “blinds” the world’s premier radio telescopes and hinders important scientific observations. It has been preferable to lose some observation time, and frequency bands, rather than draw false scientific conclusions from corrupted on-sky beampatterns. The algorithm presented here removes the effects of beampattern distortion when PSD estimation is to be performed.

For RA, modest beamshape distortions, even in the pattern sidelobes, can be unacceptable. A small pointing error or coma (teardrop distortion) in the beam mainlobe can corrupt sensitive calibrated measurements of the object brightness spatial distribution. A more subtle undesirable effect is that pattern variations in a radiometer system translate directly to an increase

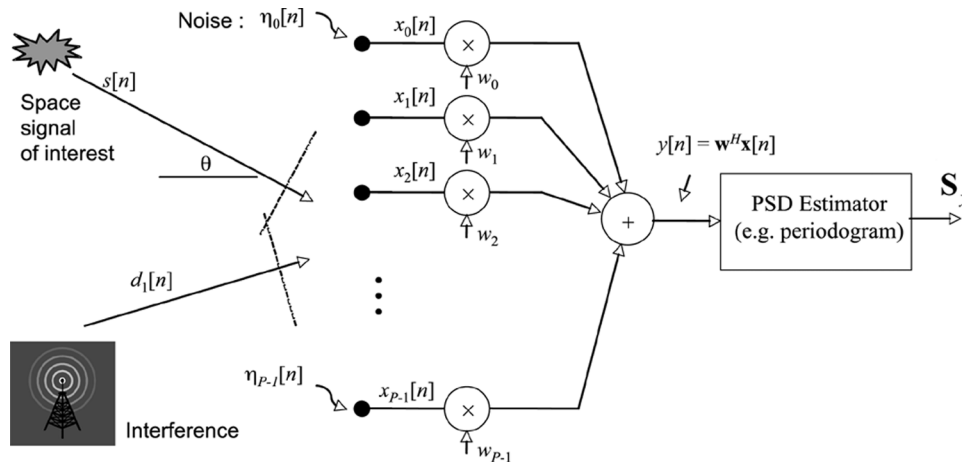


Fig. 1. Block diagram of the basic array PSD estimation system. The beamformer acts as a directional filter front-end for power spectral density estimation of the source of interest (SIO) and noise. This configuration cannot simultaneously eliminate corruption from interference and avoid bias due to adaptive interference cancellation. Fixed ground interferers appear to move relative to a deep space source due to Earth rotation.

in the minimum detectable signal level. Signals of interest can have power levels 30 dB or more *below* the noise floor. Such weak sources can only be observed by integrating the received power for a long period (seconds, minutes, or even hours) to obtain a low variance estimate of the sum of the signal and noise powers. A low variance estimate of the background noise power, obtained by switching the receiver input to a calibrated noise source or by physically steering the antenna to point away from the source, is subtracted from the signal-plus-noise estimate [17]. For spectral line (narrowband) astronomical sources, the signal may also be detectable as a spectrally nonflat perturbation of the background noise PSD. In any of these observation modes, the system response to both signal and noise must be stable to an extreme tolerance requirement over the full integration time. Variability in the antenna pattern decreases the accuracy of the noise and signal-plus-noise power estimates and as a result sensitivity is degraded. Mainlobe distortion perturbs the estimated signal power, and sidelobe variability perturbs the baseline noise power or PSD estimate. Since the noise field in radio astronomy is nonisotropic due to variations in brightness temperature of physical materials around the sensor array, or is effectively nonisotropic due to blockage by reflector antennas, even small variations in the sidelobe pattern can significantly perturb the system noise response and cause intolerable estimation bias.

In traditional, single-sensor radiometry, receiver gain fluctuation also decreases sensitivity, and sophisticated calibration schemes have been developed to achieve high stability. The pattern rumble effect described here for an adaptive array system has a similar adverse impact on sensitivity, but it is important to note that this problem is fundamentally more difficult, because pattern rumble perturbs the signal and noise responses differentially. Since the signal and noise variances are additive in their impact on the minimum detectable signal level, stable signal and noise responses are equally important.

In the radio astronomy application, interference comes from a wide range of sources, including downlink transmissions from orbiting satellites, earthbound transmissions for mobile communications, and fixed location broadcasts. Spectral bands have been reserved by international regulatory bodies for unimpeded

RA observation of important emission lines, but as astronomers seek more distant objects the associated red-shift drops these signals out of the quiet bands into a crowded spectrum. Problematic transmission reported in the literature include, among many others, the Russian GLONASS navigational satellite, the IRIDIUM satellite phone system, aircraft traffic control radar, aircraft DME navigation signals, and GSM and other mobile phone base stations [18]–[26]. As astronomers build systems for even lower frequency observation, digital television and FM radio transmissions are an issue.

We present an algorithm for correcting spectral bias in PSD estimation when using adaptive beamforming to cancel these moving, man-made interference sources. Due to Earth rotation and long integration times, even the fixed ground based emitters appear to be moving relative to a deep space object of interest, so they too satisfy the moving interference requirement. In some RA observing scenarios, deep space objects other than the SOI can be energetic enough to influence the measurements. These cannot be cancelled with the proposed algorithm because their fixed sky position exhibits no motion relative to the SOI. This is not typically an issue with array feeds on a large parabolic reflector since the dish itself provides a highly directional response which deeply attenuates space sources outside the main beam. Man-made sources, however, are often strong enough to overwhelm the dish sidelobe attenuation.

One may ask whether existing constrained adaptive beamforming methods are adequate to eliminate beampattern rumble bias in the RA PSD estimation. Classical methods include fixed-point directional constraints, derivative constraints, eigenvector constraints across a range of arrival angles, and quiescent pattern constraints [8], [9], [27]–[32]. More recently a number of promising robust adaptive beamformers have been introduced which improve constraint performance in the presence of uncertainty [33]–[36]. Each of these methods has some undesirable properties for our application. In all cases, the more extensive the constraint requirements, the more the available degrees of freedom needed for interference cancellation are reduced. None control the beampattern across all angles of arrival, which is unacceptable since for precision radiometry the entire pattern must be stable. As an example, we will demonstrate

in Section IV that fixed-point directional constraints are inadequate for PSD estimation. Robust beamformers reduce sensitivity to imprecise knowledge of the array manifold (calibration error), inaccurate SOI direction estimates, interferer subspace smearing due to motion, or sample covariance estimation error. In nonrobust classical constrained beamformers, these problems can lead to cancellation of the SOI and other instabilities. On the other hand, in our application the pattern rumble that causes PSD bias occurs even with exact calibration, perfect SOI DOA information, and exact covariance matrices, so robust methods offer no advantage. The interference canceling null itself can change noise response (in a nonisotropic field) and sidelobe pattern detail “rumbles” with interferer motion even in the robust constrained beamformers.

We propose an approach which overcomes these limitations by correcting for the averaged induced bias in the final PSD estimate rather than enforcing strict beamshape constraints while canceling time varying interference. Leshem and van der Veen introduced a bias correction method for radio astronomical synthesis imaging [2]–[4]. Radio images are formed directly from the long term integration (LTI) sample array covariance matrix, $\hat{\mathbf{R}}_x$ [37]. In Leshem’s approach, spatial filtering based on a series of tracking short term integration (STI) subspace projection operations was used to remove interference. But the projections introduced spatial covariance bias error, so a correction step was used to remove spatial bias (on average) over the full LTI.

The method of [2] can be adapted for temporal bias correction in array PSD estimation computed from the time series of an adaptive beamformer output. The resultant PSD excludes interference components and has the same effective spatial response with respect to SOI and noise as if a fixed, nonadaptive beamformer were used and no interferers were present. This is possible if the SOI is stationary while interferers move during the PSD LTI time window. It should be noted that although the LTI PSD estimate $\hat{\mathbf{S}}_y$ can be corrected for beam distortion bias, the method does not produce an unbiased beamformer time series output $y[n]$.

The paper is organized as follows. Section II introduces the mathematical models and basic algorithms used to analyze the problem. Section III describes the subspace projection adaptive beamformer approach and introduces the proposed bias correction algorithm. Algorithm bias is analyzed and an extension is developed for overlapping STI windows and window mismatch between array covariance and PSD estimators. Section IV demonstrates algorithm performance with both synthetic data simulation examples and real-world experiments. Observations and concluding remarks are found in Section V. The Appendix defines special notation, operators, and matrix algebraic identities.

II. SIGNAL MODEL AND ESTIMATION PRELIMINARIES

Consider a P element sensor array, as illustrated in Fig. 1, which at time sample n produces a length $P \times 1$ data vector

$$\mathbf{x}[n] = \mathbf{a}s[n] + \sum_{q=1}^Q \mathbf{v}_q[n]d_q[n] + \boldsymbol{\eta}[n]$$

where $s[n]$ is the SOI, $\boldsymbol{\eta}[n]$ is noise and $d_q[n]$ is one of Q “detrimental” interfering sources. Vectors \mathbf{a} and $\mathbf{v}_q[n]$ are normalized

array responses to unit amplitude point sources in the far field at directions corresponding to $s[n]$ and $d_q[n]$ respectively. Assume that $s[n]$ and $\boldsymbol{\eta}[n]$ are wide sense stationary random processes and the SOI is spatially fixed relative to the array so that \mathbf{a} is constant. On the other hand, both $\mathbf{v}_q[n]$ and $d_q[n]$ are nonstationary over the long term due to interferer motion. However, since interference motion is relatively slow compared to the sample rate, over L time samples called the “short term integration (STI)” window, the $\mathbf{v}_q[n]$ are approximately constant and the $d_q[n]$ are approximately wide sense stationary.

We define the time-dependent array autocorrelation matrix as

$$\begin{aligned} \mathbf{R}_x[n] &= E \{ \mathbf{x}[n] \mathbf{x}^H[n] \} \\ &= \sigma_s^2 \mathbf{a} \mathbf{a}^H + \mathbf{V}[n] \boldsymbol{\Sigma}_d[n] \mathbf{V}^H[n] + \mathbf{R}_\eta, \quad \text{where} \\ \mathbf{V}[n] &= [\mathbf{v}_1[n], \dots, \mathbf{v}_Q[n]] \\ \boldsymbol{\Sigma}_d[n] &= \text{diag} \left\{ \left[\sigma_{d_1}^2[n], \dots, \sigma_{d_Q}^2[n] \right] \right\}. \end{aligned}$$

Due to approximate stationarity over an STI we may write

$$\begin{aligned} \mathbf{R}_x[n] &\approx \mathbf{R}_{x,j}, \quad \forall jL \leq n < (j+1)L \\ \mathbf{R}_{x,j} &= \sigma_s^2 \mathbf{a} \mathbf{a}^H + \mathbf{V}_j \boldsymbol{\Sigma}_{d,j} \mathbf{V}_j^H + \mathbf{R}_\eta \\ \mathbf{V}_j &= \mathbf{V}[jL], \quad \sigma_{d_q,j}^2 = \sigma_{d_q}^2[jL] \end{aligned}$$

where j is the STI index. The STI sample estimator of $\mathbf{R}_{x,j}$ is computed as

$$\begin{aligned} \hat{\mathbf{R}}_{x,j} &= \frac{1}{L} \sum_{n=jL}^{(j+1)L-1} \mathbf{x}[n] \mathbf{x}^H[n] = \frac{1}{L} \mathbf{X}_j \mathbf{X}_j^H \\ \mathbf{X}_j &= [\mathbf{x}[jL], \mathbf{x}[jL+1], \dots, \mathbf{x}[(j+1)L-1]]. \end{aligned} \quad (1)$$

It is desired to estimate the temporal PSD of $s[n]$, $S_s(\omega) = \mathcal{F}(E\{s[n+m]s^*[n]\})$, without the corrupting effect of interferers $d_q[n]$ (here \mathcal{F} is the discrete-time Fourier transform with respect to m). As illustrated in Fig. 1, we use a beamformer steered to the SOI followed by a sample PSD estimator. Let the beamformer output be

$$y[n] = \mathbf{w}_j^H \mathbf{x}[n], \quad j = \lfloor n/L \rfloor \quad (2)$$

where \mathbf{w}_j is a weight vector computed for the j th STI. A basic PSD estimate can be formed from $y[n]$ using Welch’s windowed averaged periodogram [38], which can be expressed in matrix-vector form as

$$\begin{aligned} \hat{\mathbf{S}}_y &= \frac{\alpha}{M} \sum_{m=0}^{M-1} |\mathbf{F} \mathbf{G} \mathbf{y}_m|^{\odot 2}, \quad \mathbf{G} = \text{Diag}\{\boldsymbol{\gamma}\} \\ \mathbf{y}_m &= [y[m(N-O)], \dots, y[m(N-O) + N-1]]^T \end{aligned} \quad (3)$$

where N is the DFT window length, O is the number of overlapping samples in successive windows, $N \times 1$ vector $\boldsymbol{\gamma}$ is the spectral shaping time window (e.g., Hamming), $\mathbf{F} = \{(1/\sqrt{N})(e^{-i2\pi/N})^{kl}\}$ is the $N \times N$ DFT matrix where k and l are row and column indices, and $i = \sqrt{-1}$. Averaging is computed over M data windows, gross amplitude bias due to $\boldsymbol{\gamma}$ is corrected by $\alpha = 1/(\boldsymbol{\gamma}^T \boldsymbol{\gamma})$, and elements of vector \mathbf{S}_y correspond to frequency bins. To the extent that \mathbf{w}_j suppresses interferers in $y[n]$, $\hat{\mathbf{S}}_y$ is a viable estimator for $\mathbf{S}_s = \{S_s(\omega)|_{\omega=(2\pi[0,1,\dots,N-1])/N}\}$.

For RA applications $\mathbf{S}_{y,\eta} \gg \mathbf{S}_{y,s}$ element wise, where subscripts η and s denote noise and signal contributions to \mathbf{S}_y respectively. In order to estimate \mathbf{S}_s , astronomers subtract a baseline noise reference estimate computed from a separate data set with matching statistics except for the absence of signal

$$\hat{\mathbf{S}}_s = \hat{\mathbf{S}}_y - \hat{\mathbf{S}}_{y,\eta}.$$

$\hat{\mathbf{S}}_{y,\eta}$ can be obtained by temporarily steering the beam away from the source and integrating over a very long LTI widow (10 s to 10 min. or longer) to reduce estimation error variance. For an array feed operating with a large telescope reflector, this is accomplished by physically re-pointing the dish, typically by only a few beamwidths to avoid affecting the noise spectrum and to reduce the time required. Since the major source of noise field anisotropy is due to the reflector dish obscuring thermal ground noise, this re-pointing causes little change in the noise field seen by the array since the dish and array move together.

The signal spectrum can only be observed when sample error standard deviation in both $\hat{\mathbf{S}}_{y,\eta}$ and $\hat{\mathbf{S}}_y$ is below \mathbf{S}_s in all frequency bins of interest, and noise statistics have not changed during either of the LTIs used to compute them. This requires exceptional beamformer stability such that variations in \mathbf{w}_j over all j in the LTI do not affect the estimated noise power. Interferers must also be nulled in each STI to attenuate them well below the noise floor or they will dominate $\hat{\mathbf{S}}_s$.

III. BIAS CORRECTED ARRAY PSD ESTIMATION

A. Subspace Projection Adaptive Beamformer

Beamformer weights, \mathbf{w}_j , are computed using $\hat{\mathbf{R}}_{x,j}$ to track and cancel interferers while steering a high gain mainlobe toward the SOI. The beamformer must be updated each STI to satisfy

$$\mathbf{w}_j^H \mathbf{V}_j = \mathbf{0}, \quad \text{i.e. } \mathbf{w}_j \in \mathcal{N}\{\mathbf{V}_j\}$$

at least approximately, where $\mathcal{N}\{\cdot\}$ indicates nullspace. Any number of adaptive algorithms (constrained and unconstrained) can be considered, including linearly constraint minimum variance (LCMV), maximum SNR, subspace projection spatial filtering, or robust beamformers [2], [7]–[9], [22], [27]–[33], [39], but as mentioned, all will distort the quiescent (interference free) beampattern to some degree. None can simultaneously achieve deep interference nulling and beamshape control in both mainlobe and sidelobes.

We will use the subspace projection approach to form

$$\mathbf{w}_j = \mathbf{P}_j \mathbf{w} \quad (4)$$

where \mathbf{w} is a deterministic fixed beamforming weight vector with the desired quiescent beam response and \mathbf{P}_j is an estimate of $\mathbf{P}_{\mathbf{V}_j}^\perp$, the perpendicular subspace projection matrix for \mathbf{V}_j . A calibrated array is assumed so that beamforming with \mathbf{w} produces the desired pattern to within acceptable error bounds. Assuming interference dominates other signals and noise, one can use the partitioned eigen decomposition approach and let

$$\mathbf{P}_j = \mathbf{I} - \mathbf{U}_{d,j} \mathbf{U}_{d,j}^H$$

where $\mathbf{U}_{d,j}$ contains the normalized eigenvectors corresponding to the Q largest eigen values in the decomposition $\hat{\mathbf{R}}_{x,j} = \mathbf{U}_j \mathbf{\Lambda} \mathbf{U}_j^H$ such that $\mathbf{U}_j = [\mathbf{U}_{d,j} | \mathbf{U}_{s+\eta,j}]$. The number of independent interfering sources, Q , is either assumed known or is estimated using a model order estimation method such as the minimum description length algorithm [40].

B. PSD Estimator for Matched Window Sizes

When $O = 0$ and $N = L$ so the FFT windows are nonoverlapping and match the STI length, then exploiting symmetry of \mathbf{G} and \mathbf{F} and using (1), (2), and (4) in (3) yields

$$\hat{\mathbf{S}}_y^T = \frac{\alpha}{M} \sum_{j=0}^{M-1} |\mathbf{w}^H \mathbf{P}_j \mathbf{X}_j \mathbf{G} \mathbf{F}|^{\odot 2}. \quad (5)$$

Using properties 18–20 and operator definitions from the Appendix, (5) can be expressed as

$$\hat{\mathbf{S}}_y^T = \frac{\alpha}{M} (\mathbf{w}^H \otimes \mathbf{w}^T) \sum_{j=0}^{M-1} (\mathbf{P}_j \otimes \mathbf{P}_j^*) ((\mathbf{X}_j \mathbf{G} \mathbf{F}) \circ (\mathbf{X}_j \mathbf{G} \mathbf{F})^*). \quad (6)$$

The important feature of this expression is that beamformer weights have been factored out of the magnitude-squared computation, and out of the summation. Thus we can deal with the interference suppression and associated spectral bias induced by projection \mathbf{P}_j before combining the antenna signals in the beamformer. Using (1) and (2), the fixed beamforming Welch's PSD estimate (3) can be expressed in a form identical to (6) except no $\mathbf{P}_j \otimes \mathbf{P}_j^*$ term appears. Thus we identify $\mathbf{P}_j \otimes \mathbf{P}_j^*$ as a spectral bias term caused by the adaptive processing.

The special form of (6) facilitates recognizing similarities with the bias correction scheme of Leshem and van der Veen [2]–[4]. To compute an interference-free spatial array covariance estimate, they averaged over spatially filtered STI covariances

$$\begin{aligned} \hat{\mathbf{R}}_{x,\text{biased}} &= \frac{1}{M} \sum_{j=0}^{M-1} \mathbf{P}_j \hat{\mathbf{R}}_{x,j} \mathbf{P}_j^H \\ &= \text{unvec} \left\{ \frac{1}{M} \sum_{j=0}^{M-1} (\mathbf{P}_j \otimes \mathbf{P}_j^*) \text{vec}\{\hat{\mathbf{R}}_{x,j}\} \right\}. \end{aligned}$$

The bias corrected version is

$$\begin{aligned} \hat{\mathbf{R}}_x &= \text{unvec} \left\{ \frac{1}{M} \mathbf{C}^{-1} \sum_{j=0}^{M-1} (\mathbf{P}_j \otimes \mathbf{P}_j^*) \text{vec}\{\hat{\mathbf{R}}_{x,j}\} \right\}, \quad \text{where} \\ \mathbf{C} &= \frac{1}{M} \sum_{j=0}^{M-1} (\mathbf{P}_j \otimes \mathbf{P}_j^*). \end{aligned} \quad (7)$$

Following this pattern, we use (7) in (6) to form the proposed bias corrected array PSD estimator:

$$\begin{aligned} \hat{\mathbf{S}}_{y,c}^T &= \frac{\alpha}{M} (\mathbf{w}^H \otimes \mathbf{w}^T) \mathbf{C}^{-1} \\ &\quad \times \sum_{j=0}^{M-1} (\mathbf{P}_j \otimes \mathbf{P}_j^*) ((\mathbf{X}_j \mathbf{G} \mathbf{F}) \circ (\mathbf{X}_j \mathbf{G} \mathbf{F})^*) \end{aligned} \quad (8)$$

Note that here we are not computing any covariance matrix estimates (except previously to find the \mathbf{P}_j). The term under summation is essentially computing a separate interference-free PSD estimate for each receiver channel, expanded in a Kronecker product form across channels. The $(\mathbf{w}^H \otimes \mathbf{w}^T)\mathbf{C}^{-1}$ term combines the separate Kronecker channel PSDs *after* all data averaging is completed to remove bias caused by the various \mathbf{P}_j and to form the desired spatial beam response pattern.

Equation (8) is a convenient form for algorithm development and to aid analysis of the bias (see the following section) but it is not computationally efficient. The following formulation is seen by inspection to be equivalent, and is more practical for computer implementation:

$$\hat{\mathbf{S}}_{y,c}^T = \frac{\alpha}{M}(\mathbf{w}^H \otimes \mathbf{w}^T)\mathbf{C}^{-1} \sum_{j=0}^{M-1} (\mathbf{P}_j (\text{FFT}_N\{\mathbf{X}_j \circ \mathbf{\Gamma}\})) \circ (\mathbf{P}_j (\text{FFT}_N\{\mathbf{X}_j \circ \mathbf{\Gamma}\}))^* \quad (9)$$

where $\text{FFT}_N\{\cdot\}$ denotes the N point one-dimensional fast Fourier transform along matrix rows, $\mathbf{\Gamma} = \mathbf{1}_P\gamma^T$.

Since its inverse must be computed, the method requires that \mathbf{C} has a relatively low condition number (e.g., $\text{cond}\{\mathbf{C}\} < 10^4$) in order to obtain stable results for $\hat{\mathbf{S}}_{y,c}$. This is assured if there is sufficient interferer motion during the M windows of the LTI. The LTI time needed to yield a low $\text{cond}\{\mathbf{C}\}$ depends on array element spacing and aperture size, but an observation of a few tens of seconds is typically adequate for Earth rotation apparent motion of a fixed ground transmitter. Faster moving sources such as man-made satellites satisfy the requirement over much shorter LTI intervals. The computed $\text{cond}\{\mathbf{C}\}$ can be used in real-time as a switch to turn the bias correction algorithm on and off.

C. Estimation Bias Analysis

1) *Temporal-Spectral Bias:* We now present an approximation analysis showing that the proposed PSD estimator does not introduce spectral bias through its adaptive spatial processing. Assume that interferer motion is deterministic and relatively slow (e.g., satellite orbital motion) so that $\mathbf{P}_{\mathbf{V}_j}^\perp$ may be treated as deterministic under expectation and constant over an STI. Further assume that interference dominates the pre-beamforming signal environment and order estimation for Q is correct so that $\mathbf{P}_j \approx \mathbf{P}_{\mathbf{V}_j}^\perp$ with small estimation error. The random component of \mathbf{P}_j is due entirely to noise induced sample estimation error in $\hat{\mathbf{R}}_{x,j}$, which is proportional to $1/L$. This is very small relative to the deterministic part of \mathbf{P}_j which arises from interferer and array geometry. The bias of concern is due entirely to this dominant, deterministic, interference-canceling component of \mathbf{P}_j which distorts the beampatterns to cancel interference. The small sample error terms contribute only negligibly to beamshape variation. Therefore a simplifying approximate treatment assuming \mathbf{P}_j is deterministic is justified, and provides insight into the dominant characteristics of the algorithm.

Define an interference-free array data sample $\mathbf{x}_{s+\eta}[n] = \mathbf{a}s[n] + \boldsymbol{\eta}[n]$, and corresponding FFT data window matrix $\mathbf{X}_{s+\eta,j} = [\mathbf{x}_{s+\eta}[jL], \mathbf{x}_{s+\eta}[jL+1], \dots, \mathbf{x}_{s+\eta}[(j+1)L-1]]$. Accurate estimation of $\mathbf{P}_{\mathbf{V}_j}^\perp$ implies that interference components are attenuated to insignificant levels so

$\mathbf{P}_j\mathbf{X}_j \approx \mathbf{P}_j\mathbf{X}_{s+\eta,j}$. It is the product $\mathbf{P}_j\mathbf{X}_{s+\eta,j}$ which causes the undesired projection biasing of signal and noise components which must be corrected.

Taking the stated approximations into account, the expected value of the proposed estimator (8) is

$$\begin{aligned} E\{\hat{\mathbf{S}}_{y,c}^T\} &= \frac{\alpha}{M}(\mathbf{w}^H \otimes \mathbf{w}^T) \\ &\times E\left\{\mathbf{C}^{-1} \sum_{j=0}^{M-1} (\mathbf{P}_j \otimes \mathbf{P}_j^*) ((\mathbf{X}_j\mathbf{G}\mathbf{F}) \circ (\mathbf{X}_j\mathbf{G}\mathbf{F})^*)\right\} \\ &\approx \frac{\alpha}{M}(\mathbf{w}^H \otimes \mathbf{w}^T)\mathbf{C}^{-1} \left(\sum_{j=0}^{M-1} (\mathbf{P}_j \otimes \mathbf{P}_j^*)\right) \\ &\times E\{(\mathbf{X}_{s+\eta,1}\mathbf{G}\mathbf{F}) \circ (\mathbf{X}_{s+\eta,1}\mathbf{G}\mathbf{F})^*\} \\ &\approx \alpha(\mathbf{w}^H \otimes \mathbf{w}^T)E\{(\mathbf{X}_{s+\eta,1}\mathbf{G}\mathbf{F}) \circ (\mathbf{X}_{s+\eta,1}\mathbf{G}\mathbf{F})^*\} \quad (10) \end{aligned}$$

where we have substituted (7) for \mathbf{C} and exploited the wide sense stationarity of $s[n]$ and $\boldsymbol{\eta}[n]$ so dependence of $\mathbf{X}_{s+\eta,j}$ on j is removed under the expectation. This enabled factoring the summation term out of the expectation to cancel with \mathbf{C}^{-1} . Thus (10) has no dependence on adaptive canceling projection matrices, \mathbf{P}_j .

Now consider the conventional fixed beamformer PSD estimator for the case of no interference. Equation (3) can be written as

$$\hat{\mathbf{S}}_y^T = \frac{\alpha}{M} \sum_{j=0}^{M-1} |\mathbf{w}^H \mathbf{X}_{s+\eta,j} \mathbf{G}\mathbf{F}|^{\odot 2}.$$

Taking the expected value and applying matrix product properties from the Appendix leads to

$$E\{\hat{\mathbf{S}}_y^T\} = \alpha(\mathbf{w}^H \otimes \mathbf{w}^T)E\{(\mathbf{X}_{s+\eta,1}\mathbf{G}\mathbf{F}) \circ (\mathbf{X}_{s+\eta,1}\mathbf{G}\mathbf{F})^*\} \quad (11)$$

which matches (10). The important point is that given our assumptions, the bias corrected $E\{\hat{\mathbf{S}}_{y,c}^T\}$, computed in the presence of interference, has the same value as $E\{\hat{\mathbf{S}}_y^T\}$ which was computed under conditions of *no interference* and *fixed beamforming weights*. The proposed algorithm adds no pattern rumble bias. The only remaining bias terms in (10) or (11) are the well known finite length windowing effects in Welch's PSD due to \mathbf{G} , and fixed directional gain dependencies due to beamforming with \mathbf{w} .

2) *Spatial Bias:* The constant beampattern for a fixed weight conventional beamformer is

$$b(\theta) = \mathbf{w}^H \mathbf{a}(\theta) \quad (12)$$

where $\mathbf{a}(\theta)$ is the array manifold or array response vector due to a unit amplitude far field point source at θ . On the other hand, for adaptive beamformers, \mathbf{w}_j is time-varying (over j) and the instantaneous beampattern can change with each STI window in response to interferer motion.

Since $\hat{\mathbf{S}}_y$ is computed as a long-term average, we are interested in the cumulative effect of the varying \mathbf{w}_j on the directional response seen through $\hat{\mathbf{S}}_y$. We therefore define an "effec-

tive beampattern" magnitude squared directional response over the LTI as

$$|b_e(\theta)|^2 = [\hat{\mathbf{S}}_y]_{\omega=0, X_j=\mathbf{a}(\theta)\mathbf{1}_L^T} \quad (13)$$

where the subscripts indicate the PSD estimate is evaluated at baseband dc (i.e., select the first FFT bin of vector $\hat{\mathbf{S}}_y$, which corresponds to the radio frequency band center), and with sample data, \mathbf{X}_j , replaced by an $\omega = 0$, noise-free probe signal at bearing θ . In evaluating $b_e(\theta)$, all \mathbf{w}_j , and \mathbf{P}_j are first computed and stored using the observed, interference and noise corrupted data samples, \mathbf{X}_j . PSD $\hat{\mathbf{S}}_y$ is then recomputed as in (8), using these stored data dependent beamforming terms (\mathbf{w}_j and \mathbf{P}_j), but replacing \mathbf{X}_j with the angle probe signal, $\mathbf{a}(\theta)\mathbf{1}_L^T$. The effective beampattern is the angle dependent scale factor imposed by the adaptive PSD estimator, including effects of both the time varying beamforming and averaging over the LTI.

For uncorrected adaptive beamformers, assuming $L = N$, $O = 0$, and substituting (5) into (13) yields

$$|b_e(\theta)|^2 = \frac{\alpha}{M} \sum_{j=0}^{M-1} |\mathbf{w}_j^H \mathbf{a}(\theta) \mathbf{1}_L^T \mathbf{G} \mathbf{1}_L|^2 = \frac{1}{M} \sum_{j=0}^{M-1} |\mathbf{w}_j^H \mathbf{a}(\theta)|^2$$

which is simply the average over all STIs of the magnitude squared fixed beampattern for each \mathbf{w}_j . Using the bias corrected PSD, $\hat{\mathbf{S}}_{y,c}$, of (8) in (13) gives

$$\begin{aligned} |b_{e,c}(\theta)|^2 &= \frac{1}{M} (\mathbf{w}^H \otimes \mathbf{w}^T) \mathbf{C}^{-1} \\ &\quad \times \sum_{j=0}^{M-1} (\mathbf{P}_j \otimes \mathbf{P}_j^*) (\mathbf{a}(\theta) \circ \mathbf{a}(\theta)^*) \\ &= (\mathbf{w}^H \otimes \mathbf{w}^T) (\mathbf{a}(\theta) \circ \mathbf{a}(\theta)^*) = |\mathbf{w}^H \mathbf{a}(\theta)|^2 \end{aligned} \quad (14)$$

which is equal to the squared magnitude of the conventional fixed beampattern in (12). Thus the proposed algorithm removes spatial bias in the PSD estimate caused by interference canceling adaptive subspace projection beamforming. This result is easily extended to the overlapping arbitrary window size case discussed in the following section.

D. Arbitrary Window Sizes

Requiring that $O = 0$ and $N = L$ is often too restrictive for a practical PSD estimation application. Overlapping FFT windows with $O = N/2$ or $O = (3/4)N$ is common practice and improves performance when tapered windows γ (e.g., Hamming or Hanning) are used to reduce spectral leakage and sidelobe levels. Note that STI windows do not overlap. Also, the number of FFT bins, N , needed to achieve the desired spectral resolution may be smaller or larger than the length L STI window used to compute $\hat{\mathbf{R}}_{x,j}$. This is because L is tied to the interference stationarity time and so is typically independent of the desired spectral bin size. With $L \neq N$, multiple distinct beamformer weights \mathbf{w}_j may be applied across the m th N sample FFT window.

We will impose one restriction on window sizes and alignment. All STI window boundaries must fall on integer submultiples of N samples within any FFT window. Let each FFT window be partitioned into K , length N/K , subwindows such that all STI boundaries fall on some subwindow boundary. For example, if $L = 2^\nu$ where ν is an integer, $N = L/2$, and $O = L/4$, then the non overlapping STIs are twice as long as the FFT windows, which overlap by 50%. In this case $K = 2$, subwindows are $L/4$ long, and the m th FFT may be spanned by a single STI (since $L > N$) or by two STIs when an STI boundary falls at the midpoint of window m .

In this case \mathbf{y}_m in (3) becomes

$$\mathbf{y}_m = \sum_{k=0}^{K-1} \mathbf{w}_{m,k}^H \mathbf{X}_{m,k}, \text{ where}$$

$$\mathbf{w}_{m,k} = \mathbf{P}_{m,k} \mathbf{w} = \mathbf{P}_j \mathbf{w} = \mathbf{w}_j \quad \text{for } j = \left\lfloor \frac{m(N-O) + kN/K}{L} \right\rfloor$$

$$\mathbf{X}_{m,k} = \mathbf{X}_m \mathbf{J}_{m,k}$$

$$\mathbf{J}_{m,k} = \begin{bmatrix} \mathbf{0}_{kN/K} & & & \\ & \mathbf{I}_{N/K} & & \\ & & & \mathbf{0}_{N-(k+1)N/K} \end{bmatrix},$$

$$\text{such that } \sum_{k=0}^{K-1} \mathbf{J}_{m,k} = \mathbf{I}_N. \quad (15)$$

The expression for j in (15) selects the appropriate STI window (and corresponding projection \mathbf{P}_j and beamformer weight \mathbf{w}_j) which overlaps the k th subwindow of the m th FFT. Note that j can be constant over several adjacent subwindows. The two zero matrices align $\mathbf{I}_{N/K}$ in $\mathbf{J}_{m,k}$ to correspond the samples of \mathbf{X}_m which constitute the k th subwindow. Thus $\mathbf{J}_{m,k}$ is a selection matrix which zeros out all columns of \mathbf{X}_m not corresponding to subwindow k . Substituting these definitions and (4) into (3) yields

$$\hat{\mathbf{S}}_y^T = \frac{\alpha}{M} \sum_{m=0}^{M-1} \left| \mathbf{w}^H \left(\sum_{k=0}^{K-1} \mathbf{P}_{m,k} \mathbf{X}_{m,k} \right) \mathbf{G} \mathbf{F} \right|^{\odot 2}. \quad (16)$$

Using properties from the Appendix and accounting for all cross product terms among sub-windows under the magnitude square leads to an arbitrary window size version of (6)

$$\hat{\mathbf{S}}_y^T = \frac{\alpha}{M} (\mathbf{w}^H \otimes \mathbf{w}^T) \sum_{m=0}^{M-1} \sum_{k=0}^{K-1} \sum_{l=0}^{K-1} (\mathbf{P}_{m,k} \otimes \mathbf{P}_{m,l}^*) \times ((\mathbf{X}_{m,k} \mathbf{G} \mathbf{F}) \circ (\mathbf{X}_{m,l} \mathbf{G} \mathbf{F})^*). \quad (17)$$

The bias corrected PSD estimator is then

$$\hat{\mathbf{S}}_{y,c}^T = \frac{\alpha}{M} (\mathbf{w}^H \otimes \mathbf{w}^T) \sum_{k=0}^{K-1} \sum_{l=0}^{K-1} \mathbf{C}_{k,l}^{-1} \sum_{m=0}^{M-1} (\mathbf{P}_{m,k} \otimes \mathbf{P}_{m,l}^*) \times ((\mathbf{X}_{m,k} \mathbf{G} \mathbf{F}) \circ (\mathbf{X}_{m,l} \mathbf{G} \mathbf{F})^*) \quad (18)$$

where

$$\mathbf{C}_{k,l} = \sum_{m=0}^{M-1} (\mathbf{P}_{m,k} \otimes \mathbf{P}_{m,l}^*).$$

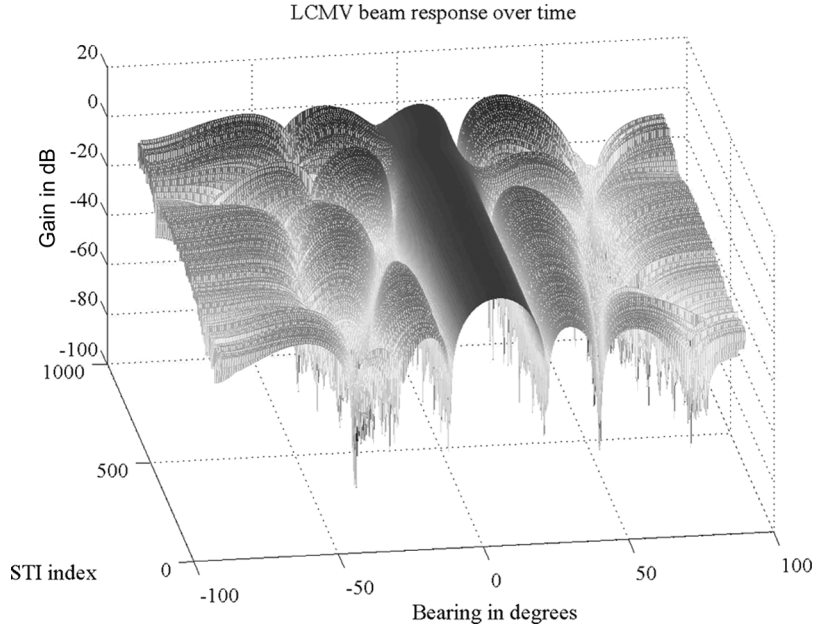


Fig. 2. Beam pattern variation over time for each \mathbf{w}_j in the LTI using the LCMV adaptive beamformer with three mainlobe constraints.

IV. RESULTS

A. Numerical Simulation Experiments

This section presents experiments using a seven element half wavelength spaced uniform line array. The source of interest was stationary, at a bearing of 5° . The true SOI PSD, \mathbf{S}_s , is seen below in Fig. 6 and consists of a narrowband CW term at $\omega = 0.4\pi$, and a structured broadband component spanning $-0.5\pi \leq \omega \leq 0.2\pi$. The broadband signal was synthesized by filtering a baseband white complex circular Gaussian random sequence with a complex 81 tap FIR multiband filter. Total power integrated across all frequencies of the broadband SOI component was 4.6 dB below total noise power, and the CW narrowband component was 39 dB below noise.

Two moving interferers were observed with initial bearings of -45° and 40° , moving at 4.9×10^{-5} and 2.5×10^{-5} degrees per sample, respectively. Both interferers were sinusoidally swept FM signals with bandwidths of 0.3π and 0.1π , at center frequencies of $\omega = -0.2\pi$ and $\omega = 0.3\pi$, respectively. Interference to noise total power ratios were 12 dB and 10 dB, so that the stronger interferer was 16.6 dB above the SOI.

All experiments except those in Section IV-A3 use the arbitrary window size algorithm of (18). This was required due to overlapping FFT windows, which also differed from the STI length of $L = 1024$ samples. FFT windows were half that size at $N = 512$ samples, and the window overlap was $O = 256$. The full LTI window includes 10^6 samples. Noise was zero mean complex Gaussian, and both spatially (across array elements) and temporally (across time samples) white.

1) *Performance Comparisons:* The synthesized data were processed with five different combined beamformer-PSD estimation methods. All but the proposed bias corrected algorithm used a conventional windowed, averaged periodogram (Welch's algorithm) at the beamformer output.

- *Fixed weight conventional beamformer.* Weight vector \mathbf{w} was set equal to the array response for a unit amplitude plane wave signal arriving from the SOI direction. This is equivalent to using the source steering vector with rectangular window shading, or the conjugate field matched beamformer. This method will not cancel interferers, but serves as a baseline for comparison with the adaptive beamformers to gauge interference attenuation, noise floor bias, and beam pattern distortion.
- *Single constraint LCMV.* A single unit magnitude response constraint is placed at the SOI direction of arrival.
- *LCMV with three mainlobe constraints.* Constraints were placed at the SOI nominal peak response direction and at the two -6 dB beamwidth points.
- *Subspace projection beamforming.* STI beamforming weights, \mathbf{w}_j were computed as in (4).
- *Bias corrected subspace projection.* This proposed method used the arbitrary sized, overlapping window formulation of (18).

Figs. 2 and 3 present the beamformer pattern evolution over time (i.e., over STI index j) produced by the three constraint LCMV and subspace projection beamformers respectively. The underlying adaptive processor in the proposed algorithm is subspace projection beamforming, so Fig. 3 also represents the instantaneous beam pattern for the new algorithm. This time variation is corrected, on average, to match a fixed conventional beam pattern. Note that in both plots, two nulls track interferer motion, cutting diagonally across the plot from left to right. For the early STIs both interferers are in the sidelobes so the mainlobe steered to 5° in Fig. 3 appears undistorted. However, in the later STIs the left-hand interferer encroaches on the mainlobe, producing significant distortion and raising the sidelobe levels. The LCMV patterns remain stable in the central mainlobe through all STIs due to the shape constraints. This seems

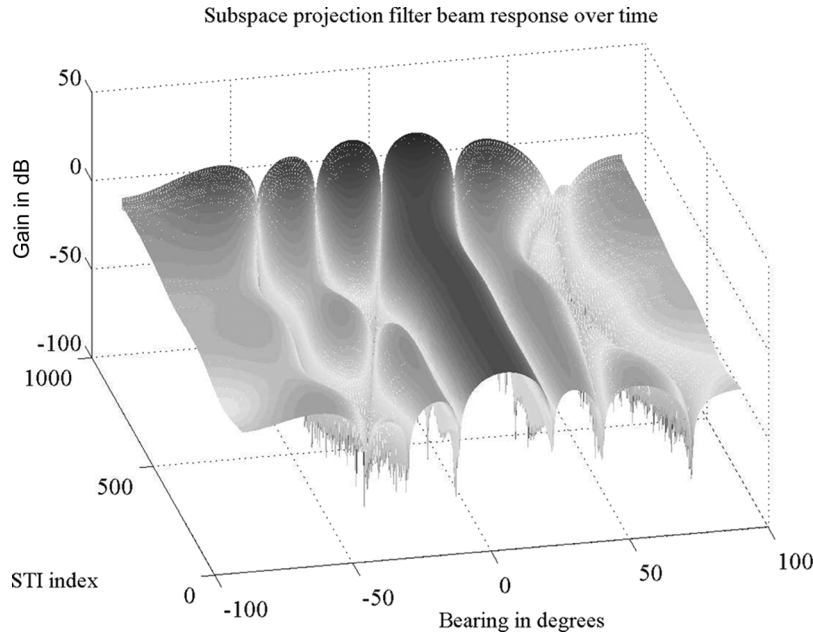


Fig. 3. Beampattern variation over time for each w_j in the LTI using subspace projection beamforming.

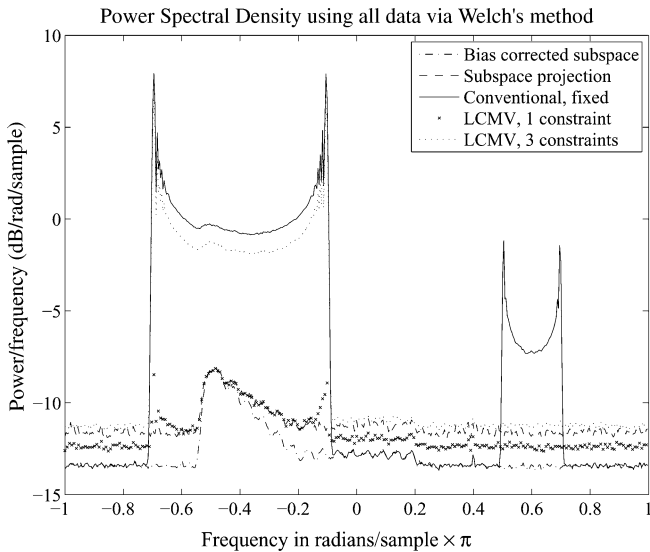


Fig. 4. PSD estimates over the full LTI. A signal of interest with spectrum shown in Fig. 6 is present, along with two broadband interferers, centered at $\omega = -0.2\pi$ and $\omega = 0.3\pi$.

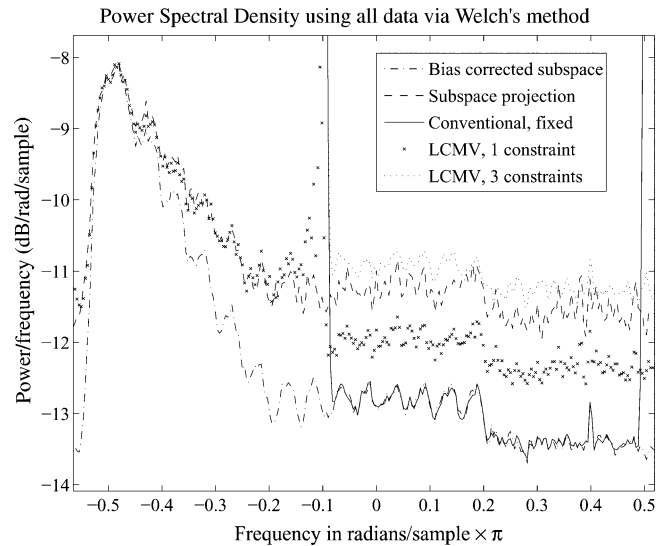


Fig. 5. Expanded view of Fig. 4 shows bias corrected PSD eliminates interference, accurately estimates signal level and structure while keeping the noise floor low.

promising, but as we will see below, the overall performance of LCMV is inadequate.

Figs. 4 and 5 show the five different resulting PSD estimates, \hat{S}_y . Curves were normalized to present equal response to the SOI so that differences in the output signal-to-noise-plus-interference ratio (SINR) are easily identified. As expected, the conventional beamformer was completely ineffective in suppressing interference, but has a low noise floor outside interference bands. Subspace projection without bias correction effectively excised interference, but due to beamshape distortions the noise floor is seen to rise. This masks weak signals of interest, like the SOI narrowband component at $\omega = 0.4\pi$, even if they are outside of the interference spectrum. In addition to a raised

noise level, increased estimation error variance introduces instability in the noise baseline estimate used in weak signal detection. Single constraint LCMV had a lower beamshape-distortion-induced noise level, but did not fully cancel the interferer. This is due to the optimization tradeoff between output noise power and interference power to achieve the minimum variance criterion. Despite the stable mainlobe of Fig. 2, the triple constraint LCMV performs very poorly overall. The interferer that spans the SOI spectrum is hardly attenuated, and the noise floor rises even higher than subspace projection.

The proposed bias corrected algorithm curves show this method maintains the low noise floor of the fixed beamformer while effectively canceling interferers. Only this curve reveals the true structure of S_s , including the low level broadband

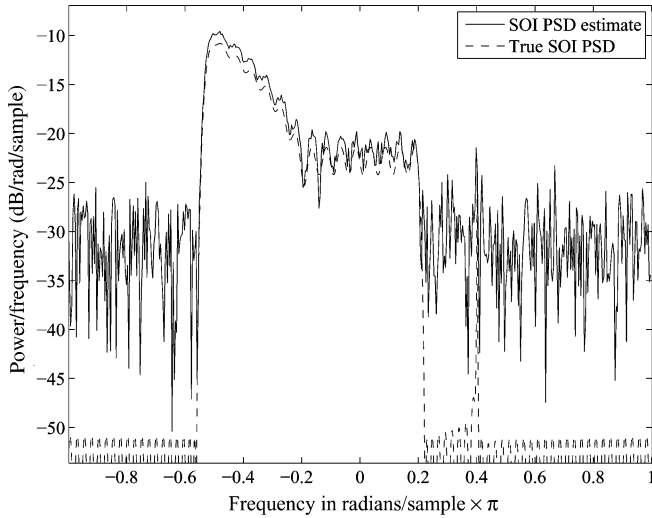


Fig. 6. Comparison of bias corrected, noise baseline removed, SOI PSD \hat{S}_s with the true S_s . Large dB deviation between the estimated and true values outside the main spectral band is due to log scale representation of the true near zero value and the sample error dominated estimate.

pedestal, the broadband ripples, and the CW narrowband component. For this simulation scenario the correction matrices were of size 49×49 , and $\text{cond}\{C_{k,l}\} \approx 140$, $0 \leq k, l \leq 1$. With this low condition number due to interferer motion over the LTI, the matrix inversion of (18) produced a stable corrected PSD estimate, $\hat{S}_{y,c}$.

Fig. 6 compares the noise-baseline-removed PSD estimate of the SOI, $\hat{S}_s = \hat{S}_y - \hat{S}_{y,\eta}$, with the true S_s . The proposed algorithm was used to compute \hat{S}_y , which is seen in the “Bias corrected subspace” curve of Fig. 4. Baseline noise estimate, $\hat{S}_{y,\eta}$, is from an independent realization of interference and noise using the same parameter settings as above, but with no SOI. The beamformer was steered to 20° to look away from the SOI direction. The match between \hat{S}_s and S_s is excellent, though due to differencing two estimators, the baseline variance doubles as expected, compared to \hat{S}_y , in Fig. 4.

Fig. 7 plots the effective beampatterns, $|b_e(\theta)|$, of the various methods. Single constraint LCMV and uncorrected subspace projection exhibit severe distortion due to adaptively canceling the interference, and thus users could not trust the PSD results to have come from the assumed directional beampattern. Though the triple constraint LCMV central mainlobe matches the fixed beamformer response, sidelobe patterns are unacceptably high. Also, no interference cancellation at all was provided as the left-most interferer moved into the mainlobe regions. The bias corrected subspace projection PSD effective beampattern, $|b_{e,c}(\theta)|$, is indistinguishable from the quiescent pattern produced by conventional fixed beamforming. This confirms the claim of beampattern bias correction in terms of its effect in the end product PSD estimate.

2) *Motion Rate Dependence*: Fig. 8 illustrates how algorithm performance degrades if interferer motion rate falls below some lower limit, or exceeds an upper bound. If motion is insufficient over the full LTI, then C is ill conditioned and cannot be inverted as required. In this case, which can be detected by computing a condition number for C , The LTI should be increased

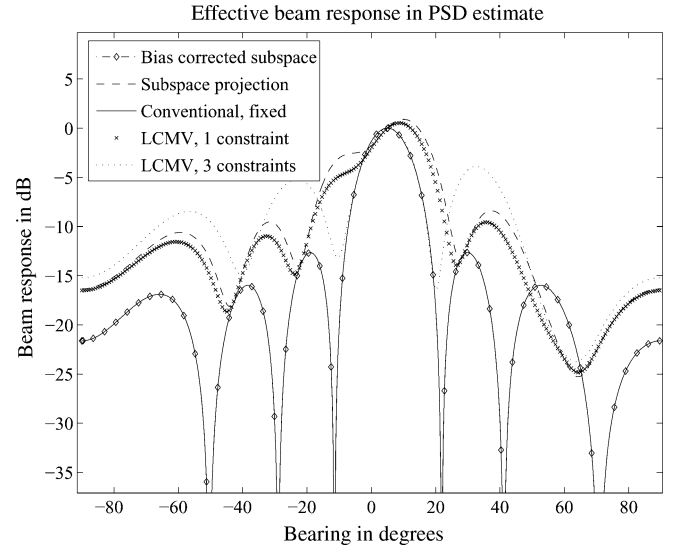


Fig. 7. Effective beam response patterns across the full LTI for each PSD estimator. Note the bias corrected subspace beamformer PSD has a completely undistorted effective beampattern, and overlays the conventional quiescent response.

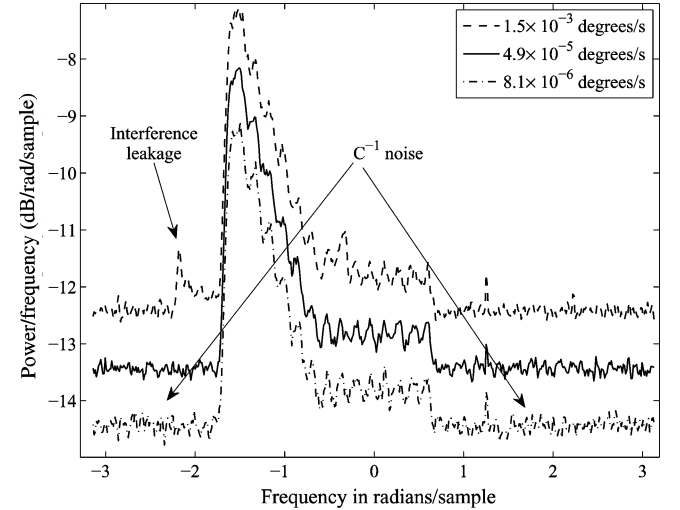


Fig. 8. Bias corrected PSD estimation performance for three interferer motion rates. Too slow motion causes instability in bias correction. Too rapid motion causes incomplete interference cancellation. Upper and lower curves are manually offset by 1 dB from the middle curve to reveal detail.

by raising M , or bias correction should be disabled. If motion is too rapid then the signal is not approximately stationary over an STI window. Subspace smearing occurs and the P_j do not fully cancel interference. In this case the STI length L should be reduced.

The actual upper and lower bounds depend on a number of factors, including motion geometry relative to array shape, array maximum aperture (distance between outermost elements), operational frequency, LTI length, L , M , and Q . Fig. 8 presents an illustrative example matching the scenario of Figs. 2–7 except that only one interferer was present (at $\omega = 0.3\pi$, beginning at bearing 45°) and its motion rate was varied. The middle curve shows baseline PSD estimation performance for a moderate motion rate of 4.9×10^{-5} degrees per second, which produced $\text{cond}\{C_{k,l}\} \approx 3.5$, $0 \leq k, l \leq 1$. Motion was reduced by small steps until noise floor instability was just noticeable at a rate of 8.1×10^{-6} degrees per second, as seen in the bottom

TABLE I
PSD ESTIMATION BIAS AND VARIANCE AT TWO FREQUENCIES

	Bias		Variance	
	$\omega = 0$	$\omega = \pi/2$	$\omega = 0$	$\omega = \pi/2$
Conventional	0.0039	209.9	0.00024	0.02838
Subspace Projection	0.2970	0.2877	0.00142	0.00156
Bias Corrected	-0.0010	-0.0098	0.00028	0.00031

curve. This is caused by a high condition number for the correction matrix, i.e., $\text{cond}\{\mathbf{C}_{k,l}\} \approx 3100$. The interferer just begins to bleed through the subspace projection filter at 1.5×10^{-3} degrees per second in the upper curve, and $\text{cond}\{\mathbf{C}_{k,l}\} \approx 3.3$. For this signal scenario and algorithm parameter settings the algorithm performs well over a range of more than two orders of magnitude in interference motion rate.

3) *Estimation Variance*: Table I presents an evaluation of variance for the proposed PSD estimator via Monte Carlo trial simulations. As above, a seven element $\lambda/2$ spaced uniform line array was used for narrowband operation with data synthesized at complex baseband and the beamformer mainlobe steered to $+5.0^\circ$. The noise floor spectrum was estimated in the presence of one strong interferer and no signal of interest. The Gaussian unit variance noise was temporally white and spatially isotropic (rather than the spatially i.i.d. noise used above). Interference was a swept FM bandpass source centered at $\omega = \pi/2$ with a bandwidth of 0.4π at an INR of $+20$ dB. Interferer motion rate was 4.85×10^{-4} degrees per sample in a zigzag pattern between -55° and $+2^\circ$, which periodically cuts into the beam mainlobe. Table I results are from 250 Monte Carlo trials, each with an LTI of length 1×10^6 samples. A different noise realization and randomized interference initial bearing angle were used for each trial. STI and FFT lengths were $L = N = 256$, nonoverlapping. Columns in the table labeled $\omega = \pi/2$ are for an FFT bin in the center of the interference spectrum, while $\omega = 0$ is a noise bin, uncorrupted by interference.

Bias is computed relative to the known true PSD for noise only (no interference) using the conventional beamformer. The conventional beamformer results show low bias and variance outside the interferer band, but it completely fails at $\omega = \pi/2$ due to high bias from the uncanceled interferer. Subspace projection exhibits moderately high bias across the band, so even frequencies outside the interference spectrum are affected. The bias corrected algorithm has very low bias and estimation variance at both frequencies, with levels on the same order achieved by the conventional beamformer at $\omega = 0$ alone.

B. Real Data Experiments

This section presents results from an experiment with a seven element L-band (≈ 1600 MHz) array feed mounted at the focal plane of a three meter diameter parabolic dish. This test platform is part of the Brigham Young University (BYU) Very Small Array (VSA) located on the roof of the engineering building. The VSA includes seven similar dishes and is used for initial experimental evaluation of signal processing algorithms for radio astronomical applications. Fig. 9 shows the antenna system and hexagonal array feed. Thickened dipole elements are used for wider bandwidth operation, and inter-element spacing of 0.6



(a)



(b)

Fig. 9. The array feed test platform. a) Feed array mounted on three meter dish reflector. b) Close-up of seven element feed.

wavelength provides a “fully sampled” array [14], [41]. Development of the BYU array is reported in [42] and [43].

The array RF front-end consists of a custom designed seven channel co-phased dual conversion receiver. Its 3.0 MHz intermediate frequency output channels are bandpass sub-sampled at 1.25 Msamples/s with synchronous 12 bit analog to digital converters. Sampled data are streamed in real time to a RAID array of high speed hard drives. This data acquisition system is capable of sampling and streaming to disc up to 20 channels, and of sample rates up to 10 Msamples/s per channel. Recorded data were post-processed in MATLAB (Mathworks, Inc.) to implement a complex basebanding digital receiver with band selection filtering and sample rate decimation for each channel. The beamforming and PSD estimation algorithms were also implemented in MATLAB.

For these experiments two RF sources with an initial apparent separation of 10° and clear lines-of-sight to the receiver dish were located on the roof of an adjacent taller building. The 3 dB full beamwidth of the dish with array feed is approximately 6° . One stationary source represented the space SOI with a low power (-110 dBm) CW narrowband tone at 1.5713 GHz. The

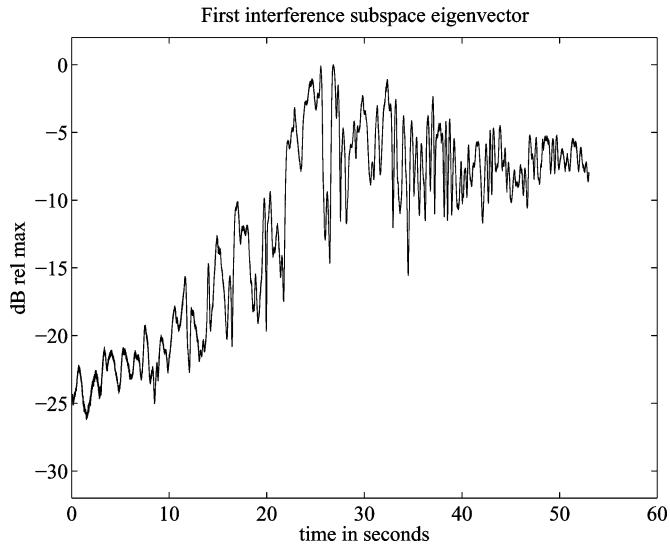
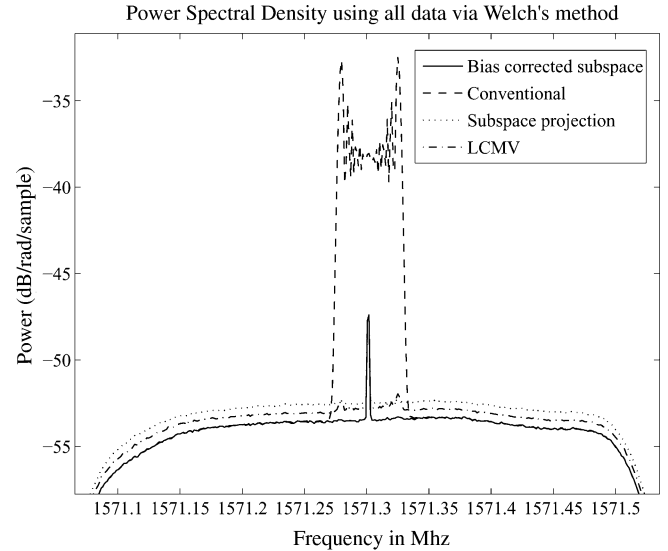


Fig. 10. Observed moving interference power at the array feed versus time. This is computed by estimating the array covariance for each successive 1024 sample data window, and then plotting the largest eigenvalue for that window. The second eigenvalue (not plotted) was relatively constant, and more than 35 dB below the peak plotted value.

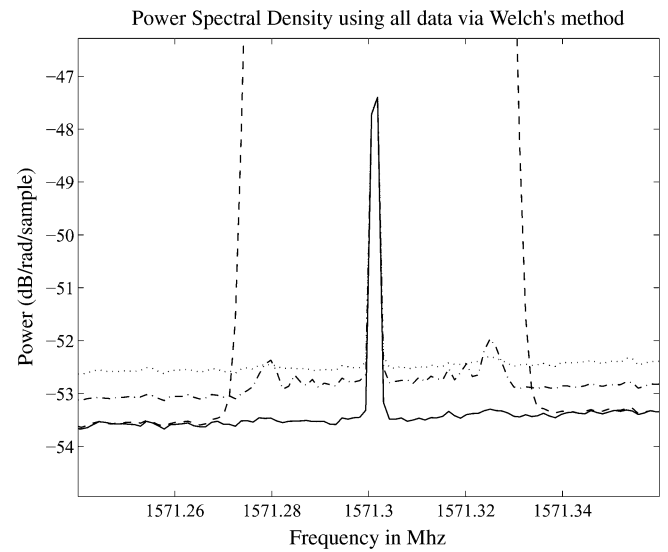
array fed receiver dish was steered to place this source in its boresight. The signal was transmitted through a calibrated standard gain horn (13 dB gain) which was aimed at the receiver dish and aligned in polarization with the array dipoles. Distance to the receiver dish was 78.5 m.

The second source represented man-made interference with an FM modulated signal, also centered at 1.5713 GHz, but with a bandwidth of 70 kHz. A handheld single dipole served as the interference transmit antenna, and motion was realized by slowly walking along the edge of the roof toward the source of interest while carrying both the signal generator and antenna. The 10° span was covered in approximately 45 seconds. Initial distance to the receiver was 87 m. A transmit power level of -35 dBm insured that interference dominated the SOI even when interference was in the dish sidelobe pattern. Fig. 10 shows the relative received interference power level over the array as a function of time, calculated as the largest eigenvalue of the array covariance matrix. Significant fine-scale fluctuations due primarily to fast multipath fading are evident. The large power increase near 22 seconds is due to the interferer entering the dish mainlobe response. This figure suggests that over any interval of a few seconds there was sufficient variation in the interference array subspace, and thus in \mathbf{P}_j , to insure that \mathbf{C} has low condition number as required by the bias correction algorithm.

Figs. 11 and 12 present performance comparisons between 1) the proposed bias corrected array PSD estimator, and Welch's PSDs computed from the outputs of three different beamformers; 2) a nonadaptive conventional beamformer; 3) the single constraint LCMV beamformer; and 4) uncorrected subspace projection as in (4). The array was calibrated in the boresight direction by observing a strong CW source with no interference and computing the resulting sample array covariance matrix, averaged over 50 ms. An eigen decomposition of this matrix was computed, and the eigenvector associated with the largest eigenvalue was taken to be the normalized



(a)



(b)

Fig. 11. PSD estimates for $t = 0$ to 15 seconds of array feed data. a) The conventional beamformer PSD fails to resolve the signal of interest (SOI) due to dominant interference. The analog receiver IF filter bandpass is seen in the shape of the noise floor. b) Detail near the SOI showing the bias corrected PSD has the same noise floor level as the nonadaptive conventional beamformer.

calibration array response, \mathbf{a} , to the SOI. We set the quiescent beamformer weight vector to $\mathbf{w} = \mathbf{a}$. Curves in Figs. 11 and 12 were normalized to have identical SOI response to remove the effect of any calibration errors in the comparisons, and to make difference in signal to noise ratios clear in the plots. Parameters N , L , O , and γ were set the same as in Sections IV-A–IV-A2.

Figs. 11 and 12 each present PSDs computed from 15 seconds of data. In both cases the SOI is completely obscured by interference when using the nonadaptive conventional beamformer, but is revealed by all three of the adaptive processors. Both the bias corrected subspace method and regular subspace projection lead to lower residual interference than LCMV. This is because LCMV devotes some degrees of freedom to reducing total variance, including noise power, instead of suppressing interference only, as with the subspace projection methods. Correction matrix condition was $\text{cond}\{\mathbf{C}_{k,l}\} \approx 4.7$

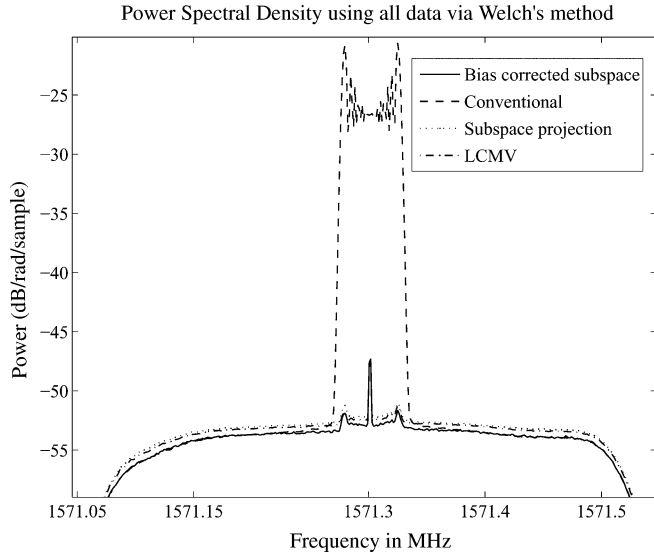


Fig. 12. PSD estimates covering $t = 15$ to 30 seconds. This time interval includes higher interference power levels (as seen in Fig. 10) due to the source entering the nominal dish beampattern main lobe. None of the cancellation methods reduced interference to the noise floor level, but the SOI is clearly observable.

and $\text{cond}\{\mathbf{C}_{k,l}\} \approx 24.9$ in Figs. 11 and 12, respectively, over $0 \leq k, l \leq 1$. This indicates more than sufficient interferer motion for bias correction. The most important feature of the plots is that without bias correction, LCMV and subspace projection have lower signal to noise-plus-interference ratios, as seen by their raised noise floors. The increased noise level is caused by beam pattern rumble due to time-varying interference cancellation. Bias corrected subspace projection has, on average over the PSD long term integration, corrected these distortions, and thus its noise floor matches that of the conventional beamformer.

V. CONCLUSION

We have introduced a new method for sensor array power spectral density estimation which eliminates the bias caused by beampattern variations arising from adaptive array interference cancellation. These biases are problematic in applications like radio astronomy where a stable spatial response pattern is as important as maximizing the instantaneous signal to interference-plus-noise ratio. Simulated and real data experiments have demonstrated algorithm effectiveness with multiple interfering sources, high interference to signal ratios, both narrowband and broadband SOIs, bare arrays with isotropic element responses, and array feeds operating at the focal plane of a reflector dish.

The method does require that interferers exhibit significant motion relative to the SOI over the PSD long-term integration timeframe, but Earth rotation in radio astronomical observing scenarios is typically adequate to meet this requirement. We also reiterate that the proposed method will not produce a bias corrected, interference cancelled beamformer output time series, but rather corrects pattern distortion bias on average over the long term integration time of a PSD estimation. A new approach would be needed, if it is even possible, to perform bias correction on a sample-by-sample basis for time-critical applications like pulsar transient analysis in radio astronomy.

For very sensitive calibrated detection and scientific measurement observations such as radio astronomy it is hoped that the proposed method will help overcome the inertia which impedes adoption of critically needed interference canceling methods. The demonstrated stability of the effective beampattern and low variance noise spectrum estimation without raising the noise floor bias are attractive features which argue for adoption in interference dominated radio astronomical observing scenarios.

We are currently preparing for experiments in conjunction with the National Radio Astronomy Observatory (NRAO) Green Bank to mount a 19 element array feed on a 20 m diameter telescope to perform PSD estimation with the proposed algorithm. This will enable performance evaluation with real-world interference as seen at the observatory in a true deep-space object observing scenario. We are also studying algorithm modifications that would permit PSD bias correction with LCMV and other adaptive array algorithms besides subspace projection. This is desirable since each algorithm performs somewhat differently, and one may be preferred over another in a particular signal scenario.

APPENDIX

The following notation, operators and identities have been used in the paper:

- 1) \mathbf{z} : bold, lower case denotes a column vector.
- 2) \mathbf{A} : bold, upper case denotes a matrix.
 $\mathbf{A} = [\mathbf{a}_1, \mathbf{a}_2, \dots, \mathbf{a}_N]$.
- 3) \mathbf{S}_x : DFT based power spectral density vector for finite length random sequence \mathbf{x}_j . This notation is an exception to rule (2).
- 4) a, B, α : italic, nonbold, Roman or Greek denotes a scalar quantity.
- 5) $\mathbf{1}_K, \mathbf{I}_K, \mathbf{0}_K$: $K \times 1$ vector of ones, and $K \times K$ identity and zero matrices respectively.
- 6) $E\{\mathbf{A}\}$: Expected value of random \mathbf{A} .
- 7) $\lfloor a \rfloor$: Floor operation, rounding toward zero.
- 8) \mathbf{A}^T : transpose of \mathbf{A} .
- 9) \mathbf{A}^* : complex conjugate of \mathbf{A} .
- 10) \mathbf{A}^H : complex conjugate (Hermitian) transpose of \mathbf{A} .
- 11) $\hat{\mathbf{A}}$: estimate of \mathbf{A} .
- 12) $|\mathbf{A}|^{\odot 2}$: element-wise magnitude squared.
- 13) $\mathbf{A} \otimes \mathbf{B} = \begin{bmatrix} a_{1,1}\mathbf{B} & \dots & a_{1,N}\mathbf{B} \\ \vdots & \ddots & \vdots \\ a_{M,1}\mathbf{B} & \dots & a_{M,N}\mathbf{B} \end{bmatrix}$, Kronecker product.
- 14) $\mathbf{A} \circ \mathbf{B} = [\mathbf{a}_1 \otimes \mathbf{b}_1, \dots, \mathbf{a}_N \otimes \mathbf{b}_N]$, Khatri-Rao product.
- 15) $\mathbf{A} \odot \mathbf{B} = \begin{bmatrix} a_{1,1}b_{1,1} & \dots & a_{1,N}b_{1,N} \\ \vdots & \ddots & \vdots \\ a_{M,1}b_{M,1} & \dots & a_{M,N}b_{M,N} \end{bmatrix}$, element-wise, or Hadamard product.
- 16) $\text{Diag}\{\mathbf{z}\}$: diagonal matrix formed with \mathbf{z} on the diagonal.
- 17) $\text{vec}\{\mathbf{A}\} = [\mathbf{a}_1^T, \mathbf{a}_2^T, \dots, \mathbf{a}_N^T]^T$ and $\text{unvec}\{\text{vec}\{\mathbf{A}\}\} = \mathbf{A}$.
- 18) $\mathbf{ABC} = \text{unvec}\{(\mathbf{C}^T \otimes \mathbf{A})\text{vec}\{\mathbf{B}\}\}$.
- 19) $|\mathbf{z}^T|^{\odot 2} = \mathbf{z}^T \circ \mathbf{z}^H$.
- 20) $(\mathbf{AB}) \circ (\mathbf{CD}) = (\mathbf{A} \otimes \mathbf{C})(\mathbf{B} \circ \mathbf{D})$.
- 21) $(\mathbf{AB}) \otimes (\mathbf{CD}) = (\mathbf{A} \otimes \mathbf{C})(\mathbf{B} \otimes \mathbf{D})$.

REFERENCES

- [1] B. D. Jeffs and K. F. Warnick, "Bias corrected PSD estimation with an interference canceling array," in *Proc. IEEE Int. Conf. Acoust., Speech, Signal Process. (ICASSP 2007)*, Honolulu, HI, Apr. 2007, vol. 2, pp. II-1145-II-1148.
- [2] A. Leshem, A.-J. van der Veen, and A.-J. Boonstra, "Multichannel interference mitigation techniques in radio astronomy," *Astrophys. J. Suppl.*, vol. 131, no. 1, pp. 355-374, 2000.
- [3] A.-J. van der Veen, A. Leshem, and A.-J. Boonstra, "Signal processing for radio astronomical arrays," in *IEEE Sensor Array Multichannel Signal Process. Workshop Proc.*, Jul. 2004, pp. 1-10.
- [4] S. van der Tol and A.-J. van der Veen, "Performance analysis of spatial filtering of RF interference in radio astronomy," *IEEE Trans. Signal Process.*, vol. 53, no. 3, pp. 896-910, Mar. 2005.
- [5] R. Klemm, *Space-Time Adaptive Processing: Principles and Applications*. London, U.K.: IEE, 1998.
- [6] S. W. Lang and J. H. McClellan, "Spectral estimation for sensor arrays," *IEEE Trans. Acoust. Speech, Signal Process.*, vol. ASSP-31, no. 2, pp. 349-358, Apr. 1983.
- [7] B. D. Van Veen and K. M. Buckley, "Beamforming: A versatile approach to spatial filtering," *IEEE ASSP Mag.*, vol. ASSP-5, no. 2, pp. 4-24, Apr. 1988.
- [8] S. P. Applebaum and D. J. Chapman, "Adaptive arrays with main beam constraints," *IEEE Trans. Antennas Propagat.*, vol. AP-24, no. 5, pp. 650-662, Sep. 1976.
- [9] R. A. Monzingo and T. W. Miller, *Introduction to Adaptive Arrays*. New York: Wiley, 1980.
- [10] K. F. Warnick and B. D. Jeffs, "Gain and aperture efficiency for a reflector antenna with an array feed," *IEEE Antennas Propagat. Lett.*, vol. 5, no. 1, pp. 499-502, Dec. 2006.
- [11] C. K. Hansen, K. F. Warnick, B. D. Jeffs, and R. Bradley, "Interference mitigation using a focal plane array," *Radio Sci.*, vol. 40, Jun. 2005, 10.1029/2004RS003138.
- [12] L. Staveley-Smith *et al.*, "The Parkes 21-cm multibeam receiver," *Pubs. Astronom. Soc. Australia (PASA)* vol. 13, p. 243, 1996 [Online]. Available: <http://www.atnf.csiro.au/research/multibeam/>
- [13] E. Ryan-Weber, B. S. Koribalski, and L. Staveley-Smith *et al.*, "The 1000 brightest HIPASS galaxies: Newly cataloged galaxies," *Astronom. J.*, vol. 124, p. 1954, 2002.
- [14] J. R. Fisher and R. F. Bradley, "Full sampling array feeds for radio telescopes," *Proc. SPIE, Radio Telescopes*, vol. 4015, pp. 308-318, 2000.
- [15] S. J. Blank and W. A. Imbrale, "Array feed synthesis for correction of reflector distortion and Vernier beamsteering," *IEEE Trans. Antennas Propagat.*, vol. AP-36, no. 10, pp. 1351-1358, Oct. 1988.
- [16] P. Shelton, "Multiple-feed systems for objectives," *IEEE Trans. Antennas Propagat.*, vol. 13, no. 6, pp. 992-994, Nov. 1965.
- [17] S. Snezana, *Single-Dish Radio Astronomy: Techniques and Applications: Proceedings of the NAIC-NRAO Summer School*. San Francisco, CA: Astronomical Society of the Pacific, 2002, NAIC-NRAO Summer School on Single Dish Radio Astronomy.
- [18] S. W. Ellingson and G. A. Hampson, "Mitigation of radar interference in L-band radio astronomy," *Astrophys. J. Suppl. Ser.*, vol. 147, pp. 167-176, 2003.
- [19] J. F. Bell, S. W. Ellingson, and J. Bunton, "Removal of the GLONASS C/A signal from OH spectral line observations using a parametric modeling technique," *Astrophys. J. Suppl.*, vol. 135, pp. 87-93, July 2001.
- [20] F. H. Briggs, J. F. Bell, and J. Kesteven, "Removing radio interference from contaminated astronomical spectra using an independent reference signal and closure relations," *Astronom. J.*, vol. 120, pp. 3351-3361, Aug. 2000.
- [21] A. J. Boonstra, A. Leshem, A.-J. van der Veen, A. Kokkeler, and G. Schoonderbeek, "The effect of blanking of TDMA interference on radio-astronomical observations: Experimental results," in *Proc. IEEE Int. Conf. Acoust., Speech, Signal Process.*, 2000, vol. 6, pp. 3546-3549.
- [22] A. Leshem and A.-J. van der Veen, "Radio-astronomical imaging in the presence of strong radio interference," *IEEE Trans. Inf. Theory*, vol. 46, no. 5, pp. 1730-1747, Aug. 2000.
- [23] W. Dong, B. D. Jeffs, and J. R. Fisher, "Radar interference blanking in radio astronomy using a Kalman tracker," *Radio Sci.*, vol. 40, no. 5, Jun. 2005, 10.1029/2004RS003130.
- [24] B. D. Jeffs, W. Lazarte, and J. R. Fisher, "Bayesian detection of radar interference in radio astronomy," *Radio Sci.*, vol. 41, Jun. 2006, 10.1029/2005RS003400.
- [25] B. D. Jeffs, L. Li, and K. F. Warnick, "Auxiliary antenna assisted interference mitigation for radio astronomy arrays," *IEEE Trans. Signal Process.*, vol. 53, no. 2, pp. 439-451, Feb. 2005.
- [26] A. J. Poulsen, B. D. Jeffs, K. F. Warnick, and J. R. Fisher, "Programmable real-time cancellation of GLONASS interference with the Green Bank telescope," *Astronom. J.*, vol. 130, no. 6, pp. 2916-2927, Dec. 2005.
- [27] H. L. Van Trees, *Detection, Estimation, and Modulation Theory, Part IV, Optimum Array Processing*. New York: Wiley, 2002.
- [28] H. Cox, "Resolving power and sensitivity to mismatch of optimum array processors," *J. Acoust. Soc. Amer.*, vol. ASSP-54, pp. 771-785, Sep. 1973.
- [29] K. M. Buckley and L. J. Griffiths, "An adaptive generalized sidelobe canceller with derivative constraints," *IEEE Trans. Antennas Propagat.*, vol. AP-34, no. 3, pp. 311-319, Mar. 1986.
- [30] M. H. Er and A. Cantoni, "An alternative formulation for an optimum beamformer with robustness capability," *IEEE Trans. Antennas Propagat.*, vol. AP-38, p. 447, Oct. 1985.
- [31] K. M. Buckley, "Spatial/spectral filtering with linearly constrained minimum variance beamformers," *IEEE Trans. Acoust., Speech, Signal Process.*, vol. ASSP-35, no. 3, pp. 249-266, Mar. 1987.
- [32] C.-Y. Tseng and L. J. Griffiths, "A unified approach to the design of linear constraints in minimum variance adaptive beamformers," *IEEE Trans. Antennas Propagat.*, vol. 40, no. 12, pp. 1533-1542, Dec. 1992.
- [33] J. Li and P. Stoica, Eds., *Robust Adaptive Beamforming*. Hoboken, NJ: Wiley-Interscience, 2005.
- [34] J. Li, P. Stoica, and Z. Wang, "On robust Capon beamforming and diagonal loading," *IEEE Trans. Signal Process.*, vol. 51, no. 7, pp. 1702-1715, Jul. 2003.
- [35] J. Li, P. Stoica, and Z. Wang, "Doubly constrained robust Capon beamforming," *IEEE Trans. Signal Process.*, vol. 52, no. 9, pp. 2407-2423, Sep. 2004.
- [36] A. B. Gershman, U. Nickel, and J. F. Böhme, "Adaptive beamforming algorithms with robustness against jammer motion," *IEEE Trans. Signal Process.*, vol. 45, no. 3, pp. 1878-1885, Jul. 1997.
- [37] G. B. Taylor, C. L. Carilli, and R. A. Perley, Eds., *Synthesis Imaging in Radio Astronomy II: A Collection of Lectures From the Sixth NRAO/NMIMT Synthesis Imaging Summer School*. San Francisco, CA: Astronomical Society of the Pacific, 1999.
- [38] P. D. Welch, "The use of fast Fourier transform for the estimation of power spectra: A method based on time averaging over short, modified periodograms," *IEEE Trans. Audio Electroacoustics*, vol. AU-15, no. 2, pp. 70-73, Jun. 1970.
- [39] S. W. Ellingson and G. A. Hampson, "A subspace-tracking approach to interference nulling for phased array-based radio telescopes," *IEEE Trans. Antennas Propagat.*, vol. 50, no. 1, pp. 25-30, Jan. 2002.
- [40] M. Wax and T. Kailath, "Detection of signals by information theoretic criteria," *IEEE Trans. Acoust., Speech, Signal Process.*, vol. ASSP-33, no. 2, pp. 387-392, Apr. 1985.
- [41] J. R. Fisher and R. F. Bradley, "Full sampling focal plane array," in *Proc. Imaging at Radio Through Millimeter Wavelength Workshop, ASP Conf. Series No. 217*, J. Mangum and S. J. E. Radford, Eds., Tucson, AZ, Jun. 1999, pp. 11-18.
- [42] J. R. Nagel, "A prototype platform for array feed development" M.S. thesis, Brigham Young Univ., Provo, UT, 2006, [Online.] Available from BYU electronic thesis collection, <http://etd.byu.edu/collection.html>, <http://contentdm.lib.byu.edu/ETD/image/etd1575.pdf>.
- [43] J. R. Nagel, K. F. Warnick, B. D. Jeffs, J. R. Fisher, and R. Bradley, "Experimental verification of radio frequency interference mitigation with a focal plane array feed," *Radio Sci.*, vol. 42, 2007, 10.1029/2007RS003630.



Brian D. Jeffs (M'90-SM'02) received the B.S. (*magna cum laude*) and M.S. degrees in electrical engineering from Brigham Young University, Provo, UT, in 1978 and 1982, respectively. He received the Ph.D. degree from the University of Southern California, Los Angeles, CA, in 1989, also in electrical engineering.

He is currently an Associate Professor in the Department of Electrical and Computer Engineering at Brigham Young University, where he lectures in the areas of digital signal processing, digital image processing, and probability theory. His current research interests include array signal processing for radio astronomy, RF interference mitigation, MIMO wireless communications, and digital image restoration. He was previously with Hughes Aircraft Company where he served as a sonar signal processing

systems engineer in the anti-submarine warfare group. His responsibilities there included algorithm development and system design for digital sonars in torpedo, surface ship towed array, and helicopter dipping array platforms.

Dr. Jeffs was a Vice General Chair for IEEE ICASSP 2001, held in Salt Lake City, UT. He was a member of the executive organizing committee for the 1998 IEEE DSP Workshop, and served several years as chair of the Utah Chapter of the IEEE Communications and Signal Processing Societies.



Karl F. Warnick (S'95–M'98–SM'04) received the B.S. degree (*magna cum laude*) with University Honors and the Ph.D. degree from Brigham Young University (BYU), Provo, UT, in 1994 and 1997, respectively.

From 1998 to 2000, he was a Postdoctoral Research Associate and Visiting Assistant Professor in the Center for Computational Electromagnetics at the University of Illinois at Urbana-Champaign. Since 2000, he has been a faculty member in the Department of Electrical and Computer Engineering

at BYU, where he is currently an Associate Professor. He has coauthored a book chapter and over 85 conference presentations and scientific journal papers, as well as a book, *Problem Solving in Electromagnetics, Microwave Circuits, and Antenna Design for Communications Engineering* (Artech House, 2006). His research interests include array antenna systems, computational electromagnetics, rough surface scattering, remote sensing, and inverse scattering.

Dr. Warnick was a recipient of the National Science Foundation Graduate Research Fellowship, Outstanding Faculty Member award for Electrical and Computer Engineering in 2005, and the BYU Young Scholar Award (2007), and served as Technical Program Co-Chair for the 2007 IEEE International Symposium on Antennas and Propagation.